Journal of Catalysis **208,** 158–169 (2002)
doi:10.1006/jcat.2002.3560, available online at http://www.idealibrary.com on IDEAL®

Acetic Acid Reduction to Acetaldehyde over Iron Catalysts

I. Kinetic Behavior

Willy Rachmady and M. Albert Vannice[1]

Department of Chemical Engineering, Pennsylvania State University, University Park, Pennsylvania 16802-4400

Received October 8, 2001; revised February 8, 2002; accepted February 8, 2002

The vapor-phase reduction of acetic acid by H_2 over both supported and unsupported iron was studied. Typical Fe catalysts increased in activity over a 4- to 5-h period to reach steady state whereas the Fe/carbon catalyst deactivated completely during this initial time on stream. The best catalysts gave selectivities to acetaldehyde between 95 and 100% at low conversions (<12%), but selectivity dropped to ~80% as conversions approached 40%. This parameter was enhanced as the H_2 pressure increased, but was almost independent of the acetic acid partial pressure. The turnover frequency for acetic acid disappearance to reduction products increased markedly from 0.003 to 0.058 s^{-1} and the apparent activation energy decreased from about 27 to 16 kcal/mol as the Fe crystallite size increased from 10 to 4000 nm. Highly dispersed 1-nm crystallites on SiO_2 exhibited no hydrogenation activity and gave only decomposition products. Acetic acid reduction over Fe is described well by a Langmuir–Hinshelwood model invoking two types of sites, i.e., one set on metallic Fe atoms that adsorbs and activates H_2, and the other on an Fe oxide surface that adsorbs acetic acid to form an acetate species. The addition of the second H atom to form acetaldehyde appears to be the rate-determining step.

INTRODUCTION

The importance of aldehydes is reflected by their broad industrial applications, whether they are used directly in flavor and fragrances or as intermediates for production of plasticizers, dyes, paints, agrochemicals, and pharmaceuticals (1). Aldehyde synthesis methods have evolved over the years as more simple and direct routes were constantly developed. Initially, Rosemund's catalytic hydrogenation of acyl chloride was widely utilized but its application was limited to small-scale practices because of the high cost associated with acyl chloride (2). A better method used lithium aluminum hydride or one of its derivatives to reduce other organics, such as esters (3–5) and carboxamides (6, 7), and carboxylic acids can also be reduced to their corresponding aldehydes using reagants such as diisobutoxyaluminum hydride (8) and thexylchloroborane-methyl sulfide [$(CH_3)_2CHC(CH_3)BHCl \cdot S(CH_3)_2$] (9). However, these synthesis methods are rather complex because of the numerous steps involved and, in addition, the reactions are stoichiometric rather than catalytic; consequently, they are impractical for industrial applications.

A synthesis method preferably should be direct and robust and applicable on an industrial scale. Catalytic oxidation of alkanes and alkenes would meet these criteria but, unfortunately, a complex reaction mixture is produced which requires additional extraction and distillation steps; thus acceptable yields of aldehydes are often lacking (10, 11). Currently, acetaldehyde is produced industrially by the Wacker process, in which ethylene is oxidized using a homogeneous $PdCl_2$–$CuCl_2$ catalyst system (12). Longer aliphatic aldehydes are produced by hydroformylation of olefins, better known as the Oxo synthesis, in which olefins react with synthesis gas (CO and H_2) to form aldehydes with one carbon atom more than the starting material (1).

Growing concerns about environmental impact, energy conservation, and process economics have called for improvements over current practices. The Wacker process requires very expensive construction materials that are resistant to the corrosive nature of the chloride-containing compounds and can safely handle the reaction. There are still efforts to optimize the Oxo synthesis to increase the yield of acetaldehyde, to reduce the high cost of separation, and to decrease the amount of unwanted by-products and waste. Reduction of carboxylic acids using molecular hydrogen offers a direct and desirable method of producing aldehydes, and very high selectivity to acetaldehyde has been achieved in acetic acid hydrogenolysis/hydrogenation over catalysts composed of Fe_2O_3, Pd/Fe_2O_3, Pt/Fe_2O_3 (13–16), Cr_2O_3 (17), and Ru–Sn (18) between 573 and 723 K. In addition, the use of a carboxylic acid as the starting material is very attractive because it can be less expensive and may be synthesized by bioprocess techniques. The high selectivity achieved with some of the above catalysts reduces the amount of unwanted by-products and the cost

[1] To whom correspondence should be addressed. E-mail: mavche@engr.psu.edu.

0021-9517/02 $35.00

of separation; therefore, this synthesis route offers the potential for a more efficient and environmentally friendly process to produce aldehydes.

Iron oxides, either with or without the presence of noble metals like Pd and Pt, have been shown to have a very good selectivity for acetaldehyde. These oxides are reducible and can form an α-Fe phase, which was proposed as one of the active phases required for the reaction between H_2 and acetic acid (HOAc) (19). The influence of small, highly dispersed metal iron particles on the kinetics of carboxylic acid reduction, however, is not yet understood. Although an early investigation found that this reaction over SiO_2-supported iron produced only acetone (20), the results reported here show that supported iron catalysts can be active for the reduction of HOAc to acetaldehyde and also have excellent selectivity. Supported iron catalysts are of special interest because they would be directly suitable to many industrial processes which are based on fixed and fluidized bed technologies. Furthermore, high surface area supports, such as SiO_2 and carbon, could provide maximum dispersion of the active phase(s). The use of supported iron catalysts for the reduction of carboxylic acids by H_2 is new, thus few quantitative studies of catalytic behavior have been conducted; therefore, the kinetic behavior of acetic acid reduction and subsequent reactions on both supported and unsupported iron was examined to enhance fundamental understanding of the mechanistic details pertaining to this reaction.

EXPERIMENTAL

Three catalysts, 3.0% Fe/SiO_2, 4.1% Fe/SiO_2, and 5.7% Fe/carbon, were prepared using an incipient wetness technique. The SiO_2 support (Davison Grade 57, 70–120 mesh, 220 m^2/g) was calcined at 773 K for 2 h under 100 cm^3(STP)/min of compressed air (MG Ind., 99.5%) to remove any organic contaminants before impregnation with an iron salt solution prepared by dissolving $Fe(NO_3)_3 \cdot 9H_2O$ (Aldrich, 99.995%) in distilled, deionized water. The carbon support—Black Pearls 2000 (Cabot Corp.)—was desulfurized for 12 h at 1223 K under 200 cm^3(STP) H_2/min (MG Ind., 99.999%) prior to impregnation with the Fe precursor solution, which was added dropwise to the support (2.2 cm^3 of solution/g of SiO_2 and 3.4 cm^3 of solution/g of carbon) with continuous stirring. One catalyst with a high Fe loading—30%Fe/SiO_2—was prepared by mixing $Fe(NO_3)_3 \cdot 9H_2O$ with silica gel while heating the mixture to the point where the ferric nitrate hydrate melted and dispersed itself over the silica (21). All catalysts prepared with water were dried in an oven at 393 K overnight in air and then stored in a desiccator. A 1.5% Fe/SiO_2 catalyst was also prepared using an incipient wetness technique, but with $Fe_3(CO)_{12}$ (Strem Chemicals) as the metal precursor and THF (Fisher Scientific, 99.9%) as the solvent. Due to the sensitivity of the metal carbonyl to oxidation, the last catalyst was prepared and dried at room temperature in a glove box purged with N_2. The final metal loading, expressed in metal weight percent, was determined by atomic absorption spectroscopy. In addition to these supported iron catalysts, Fe powder (Johnson Matthey, 99.998%) and Fe_2O_3 powder (Alfa Aesar, 99.998%) were also investigated.

The catalyst pretreatment, which normally involved reduction in flowing hydrogen at a selected temperature, was carried out *in situ* to prevent exposure of the reduced catalyst to air before its use either in a chemisorption measurement or in a kinetics experiment, and it consisted of heating at 3 K/min to 673 K under flowing H_2 (50 cm^3(STP)/min) and then holding at this temperature for 16 h. In addition to this reduction method, the 3.0% Fe/SiO_2 catalyst was also subjected to two other reduction procedures, i.e., calcination under a flowing 20% O_2–80% He mixture prior to reduction at 673 K for 16 h, and a high-temperature reduction at 723 K for 1 h. The 4.1% Fe/SiO_2 catalyst was also subjected to a high-temperature reduction at 773 K for 10 h. The Fe powder was calcined at 673 K for 1 h under a flowing 20% O_2–80% He mixture prior to the reduction treatment.

Both the supported and the unsupported Fe catalysts were characterized using H_2 and CO chemisorption, which was carried out in a stainless steel adsorption system with a base pressure of 1×10^{-6} Torr in the sample cell. H_2 (MG Ind., 99.999%) and CO (Matheson, 99.995%) were passed through a molecular sieve trap (Supelco) and an Oxytrap (Alltech Assoc.) prior to adsorption measurements, and a more detailed description of the adsorption system is given elsewhere (22). Because H_2 chemisorption on iron surfaces is inhibited at 300 K and has been found to have a maximum uptake near 373 K (23, 24), two consecutive H_2 adsorption isotherms were obtained at 373 K, which were separated by a 30-min evacuation at the same temperature. Two consecutive CO adsorption isotherms were recorded at 195 K over a range of 100–400 Torr and were also separated by a 30-min evacuation at 195 K. The iron dispersion, i.e., the ratio of surface Fe atoms to total Fe atoms ($D = Fe_s/Fe_t$), was calculated using the ratio of the total CO uptake (after correction for adsorption on the support) to the total iron loading and assuming a stoichiometry of $CO/Fe_s = 1/2$ (25). An average Fe crystallite size ($\bar{d}$) for each catalyst was then calculated using the equation (26)

$$\bar{d}(\text{nm}) = 0.75/D. \qquad [1]$$

Catalyst samples were passivated at 300 K following these adsorption measurements and then analyzed using XRD (Rigaku Geigerflex).

The kinetic behavior of vapor-phase acetic acid (HOAc) reduction by H_2 was studied using a glass microreactor

operated under differential conditions at atmospheric pressure. All lines to and from the reactor were stainless steel and were heated to 373 K to prevent condensation of any reactant or product. The total conversion of HOAc in the feed was maintained under 10% in order to minimize heat and mass transfer limitations, and this was achieved by using 50–100 mg of catalyst and a gas feed of 30 cm^3(STP)/min. Liquid acetic acid (EM Science, 99.7% Glacial) was flashed into a stream of H_2 (MG Ind., 99.999%) or He (MG Ind., 99.999%) using a syringe pump (Sage Instruments) and a preheater arm maintained at 393 K upstream from the catalyst bed. A molecular sieve trap (Supelco) and an Oxytrap (Alltech Associates) were also installed in each of the H_2 and He lines for additional purification, and flow rates were measured with mass flowmeters (Teledyne Hastings–Raydist). The composition of the product was analyzed online using a Hewlett–Packard 5890 gas chromatograph equipped with a Porapak T column (Supelco). Conversion of acetic acid was determined using a carbon balance based on the analysis of compounds detected in the effluent stream, and product selectivity was calculated based only on the carbon-containing products, which excluded the amount of water formed. The rate data were evaluated and checked using both the Madon–Boudart test (27) and the Weisz–Prater criterion (28) to ensure they were free from significant mass and heat transfer limitations.

RESULTS

H_2 and CO uptakes that were volumetrically measured at 373 and 195 K, respectively, are reported in Table 1. The adsorption isotherms are compiled elsewhere (29). The H_2 uptakes were routinely much lower than the CO uptakes and, except for 30% Fe/SiO_2 and 5.7% Fe/carbon, their values were not larger than 1.5 μmol/gcat. These low coverages of hydrogen are not unusual because hydrogen adsorption on iron is often activated (23, 24), and H_2 uptakes have been consistently lower than CO uptakes (26). Consequently, H_2 adsorption cannot be reliably used as a means of estimating the number of surface Fe atoms. Although there is no universally accepted method for estimating the number of surface Fe atoms, in general, CO chemisorption has been found to be a reasonable measure of reduced iron surface area in carbon- and MgO-supported iron catalysts (25, 26, 30). In these cases the irreversible CO uptake, i.e., the difference between the first and second isotherms, was used to estimate the number of surface Fe atoms and calculate the metal crystallite size. In the present study, however, the 3.0% Fe/SiO_2 and 4.1% Fe/SiO_2 catalysts were found to have meaningful total CO uptakes but very low irreversible uptakes. Because the CO uptake on the silica support alone was completely reversible and equal to zero when the isotherm was extrapolated to zero pressure (29), the total extrapolated CO uptake at zero pressure was associated with CO adsorbed on surface Fe atoms, and only the use of the total, rather than irreversible, CO uptake to calculate the number of surface Fe atoms provided a crystallite size in these catalysts consistent with that determined from the XRD measurement. Because the accuracy of the XRD line broadening method is reliable for this size range (31), it provided reasonable justification to use the total CO uptake to estimate iron dispersion and crystallite size. To be consistent, each turnover frequency (TOF) was calculated based on the total CO uptake in this study unless otherwise noted; consequently, this approach to normalize catalyst activity to the number of surface Fe atoms should yield a minimum value for the TOF.

A similar method was applied to the unsupported Fe powder and Fe_2O_3 catalysts. Because the XRD line broadening technique is not applicable to very large crystallite sizes (31, 32), it cannot be used to verify the chemisorption method; thus, an alternative method using an Ar BET measurement to measure the surface area of the reduced Fe powder was employed to compare it to the surface area calculated based on the total CO uptake. Assuming that the adsorption stoichiometry of CO on Fe is $CO/Fe_s = 1/2$ and the cross-sectional area of one surface iron atom is 0.094 nm^2 (33), the calculated surface area of the unsupported iron based on the total CO uptake was 0.22 m^2/g. A value of 16.7 nm^2 was used for the cross-sectional area of an Ar molecule (34), and this gave a BET surface area of 0.30 m^2/g; thus, the two methods gave reasonable agreement. The comparison was also valid for Fe_2O_3 because the oxide was essentially reduced completely to metallic iron after the reduction treatment, as evidenced by the XRD pattern and the Mössbauer spectrum obtained for this catalyst (35). The total CO uptake measured on the 5.7% Fe/carbon was not used to estimate the reduced iron surface area because a large amount of CO also adsorbed on the carbon support and the isotherms for pure carbon did not extrapolate to zero; thus, the conventional method of using the irreversible uptake was used. The iron particle size calculated with this method was consistent with that from the XRD measurement.

The influence of different pretreatments can be seen with the 3.0% Fe/SiO_2 and 4.1% Fe/SiO_2 catalysts. Calcination prior to the reduction treatment affected the total CO uptake only slightly, while a 1-h reduction at 723 K increased the total CO uptake by about 38%. The latter was more likely due to more complete reduction of very small Fe iron crystallites interacting with the silica surface. This effect was not distinguishable in the XRD measurements because the contribution from the small crystallites would be very broad and difficult to extract from the background. On the other hand, increasing the reduction temperature with 4.1% Fe/SiO_2 to 773 K lowered the CO uptake appreciably from 22 to 17 μmol/g, which implies a lower Fe surface

TABLE 1

Catalyst Characterization: CO Uptakes, Dispersions, and Average Fe Crystallite Sizes

Catalysts	Total CO uptake (μmol/g)	Irreversible CO uptake (μmol/g)	Total H_2 uptake (μmol/g)	Irreversible H_2 uptake (μmol/g)	Dispersion[a] $2[CO_{total}/Fe]$	Fe crystallite size, $\bar{d}$(nm)	
						Chemisorption[a]	XRD
1.5% Fe/SiO_2	87	37	—	—	0.64 (0.27)[b]	1.2	N.D.[c]
3.0% Fe/SiO_2[d]							
I	18	1	1	0.5	0.07 (0.004)	10.7	9
II	17	5	1.4	0.0	0.06 (0.02)	12.5	10
III	24.7	1.8	1[g]	0.6[g]	0.09 (0.007)	8.2	10
4.1% Fe/SiO_2[e]							
I	22	5	—	—	0.06 (0.01)	12.5	13
II	17	4	—	—	0.046 (0.01)	16	17
30% Fe/SiO_2	50	29	7.4	1	0.018 (0.01)	42	27
5.7% Fe/Carbon	642	77	15	3.7	1.3 (0.15)	5[f]	4
Fe_2O_3	4.2	3.5	0.8	0.0	0.0007 (0.0006)	1118	35
Fe powder	1.8	0.9	0.5	0.0	0.0002 (0.0001)	3730	45

[a] Based on total CO uptake.
[b] Numbers in parentheses denote dispersion based on irreversible CO uptake.
[c] Not detectable.
[d] I, 16-h reduction (673 K); II, 1-h calcination and 16-h-reduction (673 K); III, 1-h reduction (723 K).
[e] I, 16-h reduction (673 K); II, 10-h reduction (773 K).
[f] Based on irreversible CO uptake.
[g] At 300 K.

area in this catalyst presumably caused by sintering of the Fe particles, as corroborated by the XRD measurement.

The iron dispersion in 1.5% Fe/SiO_2, which was prepared using $Fe_3(CO)_{12}$ as the precursor, was remarkably high compared to the rest of the catalysts because there was no discernible line for Fe (or Fe oxide) in the XRD pattern obtained with the passivated catalyst. However, these well-dispersed particles of iron were expected to be oxidized completely during room temperature passivation (36), and XRD peaks arising from metallic iron were not expected.

Catalytic activity for the reduction of acetic acid by H_2 is defined here as the rate of HOAc conversion to hydrogenated products, i.e., acetaldehyde, ethanol, and ethane, and specific activity is expressed in terms of a turnover frequency (TOF), which is the activity normalized to the number of surface Fe atoms measured by CO chemisorption, i.e., molecule HOAc/($s \cdot Fe_s$). Unless noted otherwise, activity and selectivity measurements were performed at atmospheric pressure, with $P_{H_2} = 700$ Torr, $P_{HOAc} = 14.7$ Torr (H_2/HOAc = 47.6), and $T = 450$–573 K. The SiO_2 and carbon supports were inert when tested for activity under these reaction conditions.

The reaction conditions chosen to evaluate the catalytic behavior satisfied both the Weisz–Prater criterion, giving values from 0.002 to 0.08, and the Madon–Boudart test, as shown by overlapping TOFs of the 3% Fe/SiO_2 and 4% Fe/SiO_2 catalysts (see Fig. 2), because the former had 36 and the latter had 44 μmol of Fe_s/g. Although the difference in the concentration of Fe_s in the catalysts was not very large, the identical TOF values indicate the consistency of activity measurements and confirm the expected proportionality in the kinetic regime between surface Fe atoms and the measured activity showing that the kinetic data were free from mass and heat transfer limitations and other physical artifacts (27). Further evidence against any heat or mass transport effects on kinetic data is the fact that these Fe catalysts are less active under identical conditions than Pt/TiO_2 catalysts, which also passed the Madon–Boudart test (13, 29).

Figure 1 displays representative activity maintenance behavior for Fe powder, Fe/SiO_2, and Fe/carbon catalysts at 553 K. Except for Fe/carbon, which showed a dramatic deactivation within the first few hours of reaction, all supported and unsupported Fe catalysts displayed similar activity maintenance behavior, i.e., steady-state activity was typically achieved after 4–5 h on stream, it was generally higher than the initial activity, and it was maintained at the same level for up to 14 h. The products, which consisted primarily of acetaldehyde and ethanol, also varied with time on stream, and initially a higher acetaldehyde selectivity of 90–100% existed which leveled off to 80–90% acetaldehyde and 10–20% ethanol after a few hours. Fe/carbon, on the other hand, was the only catalyst that exhibited deactivation, and it was so severe that all activity was lost within the first 6 h on stream. This deactivation was also irreversible, as a short 1-h reduction treatment following deactivation gave only a slight recovery in the activity. Unlike the other catalysts, ketonization took place on Fe/carbon to yield a significant amount of acetone (~10%).

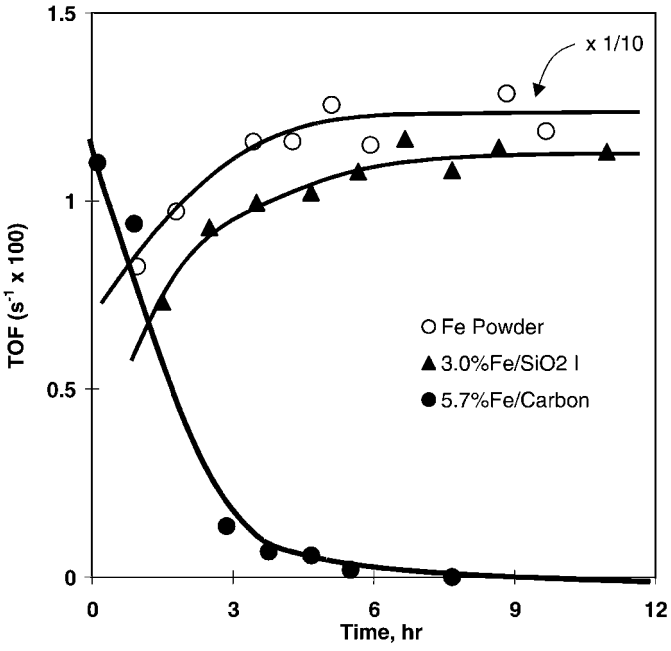

FIG. 1. Catalytic activity, expressed as a turnover frequency (molecules of HOAc/s times Fe_s), vs time on stream for Fe powder, 3.0% Fe/SiO_2 (sample I), and 5.7% Fe/Carbon. Reaction conditions: H_2/HOAc = 47.6, WHSV = 19.7 L (STP)· $g^{-1}h^{-1}$, $P = 1$ atm, and $T = 553$ K.

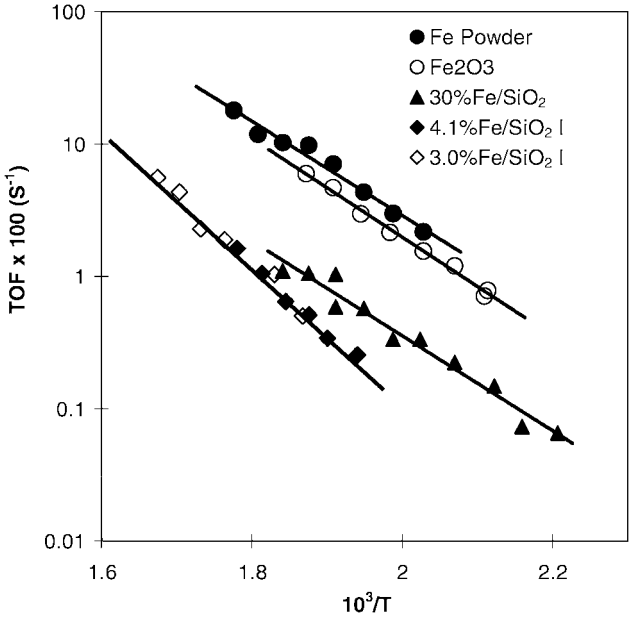

FIG. 2. Arrhenius plots of the turnover frequency for acetic acid reduction on Fe powder, Fe_2O_3, 30%Fe/SiO_2, 3.0%Fe/SiO_2 (sample I), and 4.1%Fe/SiO_2 (sample I). Reaction conditions: H_2/HOAc = 47.6, P = 1 atm.

Arrhenius plots of the reduction activity of 3.0% Fe/SiO_2 I, 4.1% Fe/SiO_2 I, Fe powder, and Fe_2O_3 are shown in Fig. 2. The activity data between 450 and 573 K were obtained under both increasing and decreasing temperature conditions after steady-state conditions were achieved in order to verify the reproducibility of the measurements and to detect if any deactivation occurred. Apparent activation energies obtained from the slopes of the Arrhenius plots varied between 16 and 27 kcal/mol, as shown in Table 2, and activities at 523 K showed a significant disparity in TOF among the supported and unsupported iron catalysts. The well-dispersed 1.5% Fe/SiO_2 catalyst, which was prepared with $Fe_3(CO)_{12}$, showed negligible reduction activity and the reaction yielded only acetone and CO_2. A moderately dispersed 6% Fe/carbon catalyst, on the other hand, had a substantially higher initial TOF but it deactivated very rapidly, which prevented measurement of its steady-state activity and activation energy.

Different pretreatments also affected the kinetics, as seen with 3.0% Fe/SiO_2 and 4.1% Fe/SiO_2. A calcination treatment of 3.0% Fe/SiO_2 II prior to the standard reduction procedure increased the TOF significantly. A 1-h reduction of 3.0% Fe/SiO_2 III at 723 K, which increased the Fe_s concentration, produced a TOF similar to that of the catalyst pretreated with the standard reduction, whereas reduction of 4% Fe/SiO_2 II at 773 K produced larger Fe crystallites but also increased the TOF. The large Fe crystallites in the 30% Fe/SiO_2 catalyst had the highest TOF and lowest activation energy of the supported Fe catalysts. Unsupported iron derived from Fe_2O_3 or Fe powder was very active for hydrogenolysis and hydrogenation, as exhibited by TOFs that were an order of magnitude larger than those of the supported catalysts, while their apparent activation energies were similar to that of 30% Fe/SiO_2.

With the exception of the 6% Fe/carbon and 1.5% Fe/SiO_2 samples, very high acetaldehyde selectivity was

TABLE 2

Activities and Apparent Activation Energies for Acetic Acid Reduction by H_2 over Fe Catalysts

Catalysts	Reduction activity at 523 K: μmol HOAc/s/gcat	Reduction activity at 523 K: μmol HOAc/s/g Fe	TOF at 523 K ($s^{-1} \times 100$)	Activation energy (kcal/mol)
1.5% Fe/SiO_2	0.0	0.0	0.0	—
3.0% Fe/SiO_2				
I	0.12	4.0	0.33	24
II	0.18	6.0	0.53	27
III	0.16	5.3	0.32	24
4.1% Fe/SiO_2				
I	0.15	3.7	0.34	24
II	0.25	6.1	0.74	21
30% Fe/SiO_2	0.83	2.8	0.83	17
5.7% Fe/Carbon	1.7[a]	30[a]	1.1[a]	—
Fe_2O_3	0.35	0.18	4.2	17
Fe powder	0.21	0.21	5.8	16

[a] Initial activity at 553 K. $P_{HOAc} = 14$ Torr; $P_{H_2} = 700$ Torr.

TABLE 3

Product Selectivity during Acetic Acid Reduction

Catalyst	Temp (K)	Conversion %	Selectivity (mol%)					
			Acetaldehyde	Ethanol	Ethane	Ester	Acetone	$CH_4 + CO_2 + CO$
1.5% Fe/SiO_2	616	4	0	0	0	0	50	50
3.0% Fe/SiO_2	533	4	100	0	0	0	0	0
	543	8	90	7	0	4	0	0
4.1% Fe/SiO_2	518	3	90	6	0	0	2	2
	550	8	90	2	0	0	4	4
30% Fe/SiO_2	453	2	100	0	0	0	0	0
	503	11	95	5	0	0	0	0
5.7% Fe/Carbon	553	5	64	11	0	3	11	11
Fe_2O_3	503	4	100	0	0	0	0	0
	533	12	95	5	0	0	0	0
Fe powder	493	5	100	0	0	0	0	0
	513	10	94	6	0	0	0	0

generally obtained with iron catalysts, and Table 3 shows product distributions obtained at steady state. Selectivities as high as 100% were obtained at conversions of 5% and below, but higher conversions shifted the product distribution to ethanol, one of the secondary reduction products. In addition to ethanol, ethyl acetate was also produced at high conversions. The effect of conversion on product selectivity can be seen more clearly in Fig. 3, which shows that an increase in conversion to 35% decreased acetaldehyde selectivity to 80%. The maximum conversion obtained here is about one-half the equilibrium conversion of 80% under standard reaction conditions. The effect of temperature can be excluded from this selectivity profile because the conversion was varied by changing the space velocity at a constant temperature of 523 K. Ethane, methane, and carbon monoxide were detected in much smaller amounts (5–6%), but usually only at temperatures above 553 K. Significant ketonization activity was observed with 1.5% Fe/SiO_2 and 5.7% Fe/carbon, which yielded acetone and CO_2, and in fact, this was the only activity observed with 1.5% Fe/SiO_2.

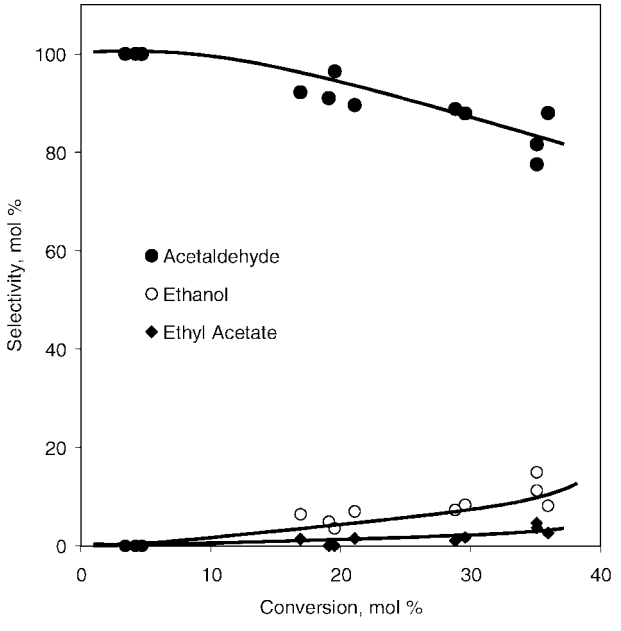

FIG. 3. Product selectivity as a function of acetic acid conversion over silica-supported iron catalysts at 523 K.

The effect of reactant partial pressure on reaction kinetics was also determined using 4.1% Fe/SiO_2. Catalytic activities were first measured at hydrogen partial pressures between 100 and 700 Torr while the HOAc partial pressure was kept constant at 14.3 Torr, then HOAc partial pressures were varied between 3 and 54 Torr while the H_2 partial pressure was kept constant at 700 Torr. Data were obtained at three different temperatures between 530 and 568 K and, for each data set, activity measurements were made at both increasing and decreasing partial pressures to verify the reproducibility of the measurement. In addition, the rate measurements at $P_{H_2} = 700$ Torr and $P_{HOAc} = 14.3$ Torr were compared for consistency with those obtained during separate Arrhenius runs conducted at these standard conditions. These results, when interpreted by a power rate law, showed that the apparent reaction order with respect to hydrogen varied between 1 and 2 while that with respect of acetic acid remained near zero, as indicated in Table 4. While the change in HOAc partial pressures had insignificant effect on the product distribution, acetaldehyde selectivity was markedly affected by the H_2 partial pressure, as shown in Fig. 4, and lower pressures of H_2 increased acetone formation significantly.

DISCUSSION

There are various reactions involving acetic acid that can occur over metal and metal oxide surfaces. The reduction

TABLE 4

Apparent Reaction Orders with Respect to H_2 and Acetic Acid (HOAC) Partial Pressures for Acetic Acid Reduction over 4.1% Fe/SiO_2

	Reaction Order	
Temp. (K)	x	y
530	0.08	1.1
546	0.06	1.4
568	0.09	1.7

Note. The rate of reaction is expressed as $r_{HOAc} = k P_{HOAc}^{x} P_{H_2}^{y}$.

pathway consists of an initial hydrogenolysis step involving the addition of one molecule of hydrogen to HOAc to produce water and acetaldehyde, which can then be further hydrogenated to ethanol and then reduced to ethane. The latter reactions are particularly rapid on Pt/TiO_2 and Pt/Al_2O_3 (13). An important secondary reaction pathway is esterification involving HOAc and the hydrogenation product, ethanol, and it becomes particularly important when the ethanol concentration is high, typically at high conversions. A bimolecular HOAc ketonization reaction to produce acetone along with CO_2 and water can also be significant in the absence of, or at low partial pressures of, hydrogen, particularly on metal oxides such as Al_2O_3, Fe_2O_3, TiO_2 (13), and others, as reported by Pestman and coworkers (37a, 37b). Dehydration of HOAc to form ketene can also occur on metal oxides, and although ketene formation is rarely observed at atmospheric pressure or higher, ketene production can occur with short contact times over functionalized silica monoliths (38). Finally, HOAc can also decompose via decarboxylation and decarbonylation pathways to produce CH_4, CO, CO_2, and water. These reactions are typically associated with metal surfaces but require much higher temperatures than hydrogenation and ketonization reactions. The products of these reactions are depicted in Table 3.

The reduction of HOAc by H_2 to acetaldehyde is certainly favorable on iron-based catalysts, as reflected by their selectivities above 80%, and is in sharp contrast to Pt/TiO_2. Given that acetaldehyde, ethanol, and ethane are the products of consecutive reactions involving hydrogen, the high selectivity to acetaldehyde on these catalysts implies a higher rate of acetaldehyde desorption from iron surfaces relative to its further hydrogenation to ethanol. It can also imply that the adsorption of acetic acid is more favored than that of acetaldehyde.

Another unique feature of these reduced iron catalysts is that they generally require an induction period of up to 5 h on stream to achieve stable behavior, except for the Fe/carbon catalyst, which showed severe deactivation during this period. It has been proposed that both metal and oxide phases are required for HOAc reduction over supported Pt and Fe_2O_3 (13, 19, 37), and the same criterion should also apply to these iron catalysts. Due to its strong oxidizing nature, HOAc should be capable of oxidizing some of the metallic surface iron atoms after adsorption. After reduction most, if not all, of the iron is in the metallic phase

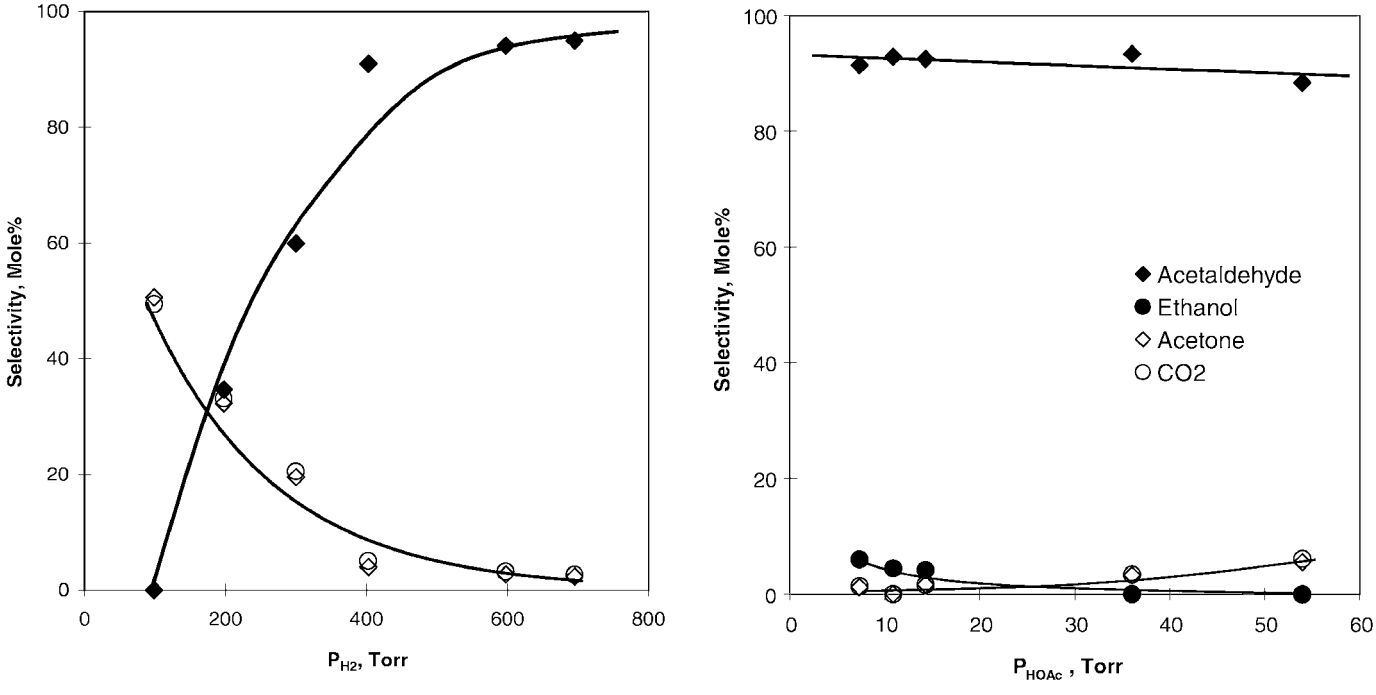

FIG. 4. Product distribution as a function of hydrogen and acetic acid partial pressures using 3.0% Fe/SiO_2 at 568 K and ~10% conversion.

and some time would be required for conversion into a bulk oxidic phase; thus, this induction period may be associated with the transformation into a mixed-phase state consisting of zero-valent iron and iron oxide. The former is required to activate H_2 by dissociative adsorption, while the latter is needed to activate acetic acid.

Apparent activation energies can be an important indicator of kinetic behavior because they can be composite values representing a number of elementary steps, including adsorption of HOAc and hydrogen; however, the exact relationship among these entities is often nonlinear and complex, depending on the intrinsic kinetics. Acetic acid reduction over supported Pt catalysts exhibited activation energies from 9 to 13 kcal/mol (13), whereas the values obtained for iron catalysts were generally twice as much, i.e., between 17 and 27 kcal/mol; thus, the large differences in E_a values can imply that the reaction proceeds via a different mechanism on these two catalysts; for example, a different rate-determining step (rds) could occur in the same sequence of elementary steps. On the other hand, if the reaction occurs via the same mechanism and the same surface species are assumed to predominate in these two catalyst systems, the larger apparent activation energy associated with iron catalysts could be related to a lower heat of adsorption for HOAc and/or hydrogen on Fe compared to Pt. Unfortunately, the heat of adsorption for acetic acid on either metal surface is not known, so a direct comparison is not possible. In contrast, hydrogen adsorption on Pt and Fe surfaces has been studied extensively and markedly different behavior has been observed in that values for the heat of adsorption of H_2 on reduced iron surfaces have varied between 23 and 39 kcal/mol (39–43) while those for Pt are lower and have ranged from 9 to 29 kcal/mol (44). However, hydrogen adsorption on Fe is very sensitive to surface contamination and it often becomes an activated process (45, 46).

Both the turnover frequency (TOF) and the apparent activation energy (E_a) are affected by iron crystallite size. As displayed in Fig. 5, as the average iron crystallite size increased from 10 to 4000 nm the TOF increased from 0.3 to 6 s^{-1} and the E_a value decreased from 27 to 17 kcal/mol. A dependency of catalytic properties on iron particle size has been observed previously in both the ammonia synthesis (23, 47) and the hydrocarbon synthesis (48) reactions. For example, the TOF for ammonia synthesis increases several orders of magnitude as the iron particle size varies from 1 to 30 nm, and Topsøe and coworkers have reasoned that this behavior is caused by an increase in the concentration of active sites on the surface as the iron particle size increases (23). Although the influence of iron particle size on the TOF for HOAc reduction is not as significant as that mentioned above, the trend is similar. Furthermore, the Fe particle size range in this study falls outside that which should alter the behavior of "structure-sensitive" reactions most dramatically, i.e., 1–5 nm (49); therefore, the extent of the crystallite size effect must be considered to be incompletely determined at this time.

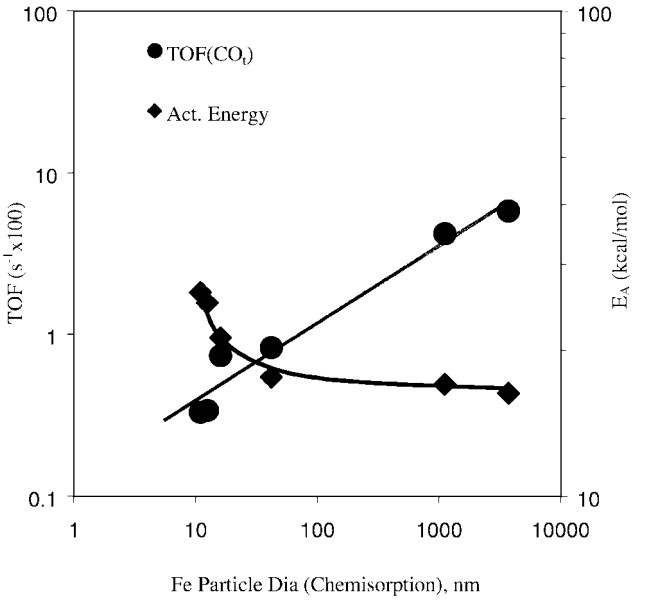

FIG. 5. Effect of Fe particle size on turnover frequency (based on total CO uptake) and activation energy.

The activity trend observed during the catalytic activity maintenance study, as displayed in Fig. 1, indicates transient behavior during the first 4–5 h, during which dynamic restructuring of iron occurred due to oxidation and re-reduction by the reactants to leave mixed-phase iron, as discussed in the second part of this study (35). The presence of both metallic and oxidic Fe phases facilitates this reaction, and the respective amounts of these two surface iron phases dictate the kinetics. Iron surfaces are highly susceptible to oxidation, but the degree of oxygen removal from the surface during re-reduction has been found to vary from one Fe surface to another (50, 51), and it can vary with iron particle size (46); thus, the thermochemical quasiequilibrium of iron phases present under a particular gas-phase composition in the catalyst bed may vary with iron particle size, but to what extent is presently unknown. Based on the evidence that the attainable degree of reduction increases with increasing iron particle size (35), one might speculate that the fraction of surface maintained in the metallic form increases as crystallite size increases. With very small iron particles, such as in the case of 1.5% Fe/SiO_2, the iron cannot be reduced to the zero-valent state under the pretreatment and reaction conditions employed here (35), thus causing the lack of hydrogenation activity observed. Hydrogen chemisorption can also be affected by the presence of oxygen on the surface, and it is a slow and activated process on small iron particles when oxygen is not easily removed (46); consequently, one might surmise that the energy associated with hydrogen adsorption may also vary with particle size and alter the apparent activation

energy. Subsequently, the increase in TOF and the decrease in E_a may also be attributed to varying degrees of iron reduction and hydrogen adsorption on these surfaces under reaction conditions.

A previous kinetic study of acetic acid reduction by H_2 over Pt/TiO_2 catalysts showed that the reaction can be described by a Langmuir–Hinshelwood-type mechanism invoking two types of sites, one on the metal to activate H_2 and the other on the oxide to adsorb and activate HOAc (13). A TPD and DRIFTS study of HOAc adsorbed on Pt/TiO_2 provided evidence that reduction of HOAc proceeds predominantly via addition of atomic hydrogen to an acyl species which is formed when HOAc adsorbs on the titania surface (52). Acetaldehyde is the initial product, and it can either desorb or react with additional hydrogen atoms to form ethanol and, subsequently, ethane. The proposed reaction mechanism consisted of quasiequilibrated hydrogen and HOAc adsorption, two irreversible elementary surface reactions steps, and reversible product desorption steps, which allowed the derivation of a rate expression that exhibited thermodynamic consistency and fit with the experimental data well (13, 52).

This current investigation of iron catalysts indicates that the reaction over these catalysts can again involve a metallic phase of iron to activate H_2 and an oxidic phase to activate acetic acid, and optimal reduction performance is obtained when both phases are present. Despite this similarity between iron and Pt/TiO_2 catalysts, the intrinsic kinetic behavior is different, as indicated by the results obtained with 4% Fe/SiO_2, i.e., the apparent reaction order with respect to the hydrogen partial pressure is between 1 and 2 and more than double that obtained for Pt/TiO_2, the rate has no dependence on the HOAc partial pressure, and the apparent activation energy is twice that for Pt/TiO_2. Regardless, a reaction model similar to that used to describe HOAc reduction over Pt/TiO_2 was applied to this reaction over 4%Fe/SiO_2, with the only difference being that the rds involved the addition of the first H atom to an acetate species rather than an acyl species, based on DRIFTS, TPD, and TPR results (35). However, the rate expression derived from this model had a maximum reaction order on H_2 pressure of unity, whereas the experimental values obtained here were greater than 1, as shown by the slopes of the ln TOF vs ln P_{H_2} plots in Fig. 6. In addition, analysis of the entropy of adsorption for H_2, obtained from the equilibrium adsorption constants in the rate expression, gave a value much higher than the absolute entropy of H_2. Consequently, these considerations led to rejection of this model (29).

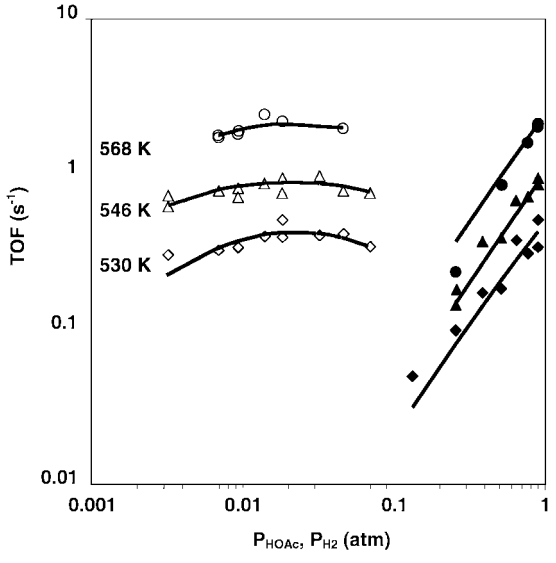

FIG. 6. Dependence of kinetic behavior of 4.1%Fe/SiO_2 on acetic acid and hydrogen partial pressures. Solid lines denote the optimum fits from Eq. [16] while the open symbols are data obtained at constant P_{H_2} and the filled symbols are data obtained at constant P_{HOAc}.

However, the higher reaction order can also imply that addition of the first hydrogen atom to the adsorbed acetate species is a rapid, quasiequilibrated step, which would give the following sequence of elementary steps to describe this reaction on iron:

$$H_{2(g)} + 2^* \overset{K_H}{\rightleftharpoons} 2H^*, \quad [2]$$

$$CH_3COOH_{(g)} + 2^* \overset{K_{Ac}}{\rightleftharpoons} CH_3COO^* + H^*, \quad [3]$$

$$CH_3COOH_{(g)} + S \overset{K_A}{\rightleftharpoons} CH_3COOH\text{-}S, \quad [4]$$

$$CH_3COOH\text{-}S \overset{K_{Ace}}{\rightleftharpoons} CH_3COO\text{-}S\text{-}H, \quad [5]$$

$$CH_3COO\text{-}S\text{-}H + H^* \overset{K_1}{\rightleftharpoons} CH_3CHO\text{-}S\text{-}OH + {}^*, \quad [6]$$

$$CH_3CHO\text{-}S\text{-}OH + H^* \xrightarrow{k_2} CH_3CHO\text{-}S + {}^* + H_2O_{(g)}, \quad [7]$$

$$CH_3CHO\text{-}S \underset{k_{-3}}{\overset{k_3}{\rightleftharpoons}} CH_3CHO_{(g)} + S, \quad [8]$$

$$CH_3CHO\text{-}S + H^* \xrightarrow{k_4} CH_3CHOH\text{-}S + {}^*, \quad [9]$$

$$CH_3CHOH\text{-}S + H^* \xrightarrow{k_5} CH_3CH_2OH\text{-}S + {}^*, \quad [10]$$

$$CH_3CH_2OH\text{-}S \underset{k_{-6}}{\overset{k_6}{\rightleftharpoons}} CH_3CH_2OH_{(g)} + S, \quad [11]$$

where $*$ and S represent sites on the metallic and oxidic iron phases, respectively, and the latter type of site could involve more than one atom. As mentioned, the reduction activity represents only the formation of acetaldehyde, ethanol, and ethane, and application of the steady-state approximation to the surface intermediates with the assumption that the product partial pressures, and hence their surface concentrations, are very low gives a reaction rate of

$$r_{HOAc} = k_2\theta_{AH}\theta_H, \quad [12]$$

where θ_i is the fractional surface coverage of species i, and the subscripts AH and H refer to the partially hydrogenated

acetate species on the oxidic sites, S, which exist in the interfacial region between the metallic and oxidic phases, and hydrogen atoms on the metallic sites, $*$, respectively.

Assuming that adsorbed hydrogen atoms (H^*) and an acetate species (CH_3COO^*) are the abundant surface species on metallic Fe sites and that the $*$ sites are near saturation coverage, a balance on the $*$ sites gives the following expression for θ_H:

$$\theta_H = \frac{K_{H_2}^{1/2} P_{H_2}^{1/2}}{\left(K_{H_2}^{1/2} P_{H_2}^{1/2} + K_{Ac} P_A / K_{H_2}^{1/2} P_{H_2}^{1/2}\right)}. \quad [13]$$

It is further assumed that a surface acetate species (Ace) is the most abundant surface intermediate on the S sites, an assumption supported by the low conversions (hence low product concentrations) and by DRIFTS spectra obtained during reaction over 3.0% Fe/SiO_2, which are shown in the second part of this series (35). This gives the following equation for θ_{Ace}:

$$\theta_{Ace} = \frac{K_{Ace} K_A P_A}{(1 + K_{Ace} K_A P_A)}. \quad [14]$$

Then $K_1 = \dfrac{\theta_{AH}\theta_*}{\theta_{Ace}\theta_H}$ to give

$$\theta_{AH} = K_1 \theta_{Ace} \theta_H / \theta_*, \quad [15]$$

where θ_* represents the fraction of vacant metallic sites, and the final rate expression is obtained by substituting Eqs. [13]–[15] into Eq. [12] to give

$$r_{HOAc} = \frac{k_2 K_1 K_{Ace} K_A K_{H_2} P_A P_{H_2}}{\left(K_{H_2}^{1/2} P_{H_2}^{1/2} + K_{Ac} P_A / K_{H_2}^{1/2} P_{H_2}^{1/2}\right)(1 + K_{Ace} K_A P_A)}$$

$$= \frac{k P_A P_{H_2}^{3/2}}{(K_{H_2} P_{H_2} + K_{Ac} P_A)(1 + K_{Ace} K_A P_A)}, \quad [16]$$

in which the total number of $*$ and S sites is incorporated into k. Based on this rate equation, the maximum possible reaction order with respect to acetic acid can vary between -2 and unity, but the maximum with respect to H_2 pressure is now 1.5. Other models were considered but rejected on the basis of inadequate fit or inconsistent thermodynamic parameters (29).

The rate equation given by Eq. [16] was fitted to the experimental data obtained from the partial pressure runs with 4.1% Fe/SiO_2 using a least-square nonlinear optimization method. An iteration method was performed using the Microsoft Excel Solver Routine, and the process was initiated with various sets of initial values and continued to verify that the same set of optimum values was obtained. These optimum parameters are given in Table 5. The equilibrium adsorption constants found in Eq. [16] can be written as

$$K_i = \exp\left(\Delta S_{ad,i}^0 / R - \Delta H_{ad,i}^0 / RT\right), \quad [17]$$

TABLE 5

Optimized Rate Parameters for Acetic Acid Reduction over 4.1% Fe/SiO_2[a]

Temp (K)	$K_1 k_2$ ($s^{-1} \cdot atm^{-2}$)	$K_{H_2} \times 10^{-3}$ (atm^{-1})	$K_{Ac} \times 10^{-6}$ (atm^{-1})	$K_{Ace} K_A$ (atm^{-1})
530	0.044	32.6	4.48	12.2
546	1.03	5.38	2.06	5.51
568	1.59	3.63	0.87	7.11

[a] In Eq. [16].

where R is the ideal gas law constant, T is temperature, and $\Delta S_{ad,i}^0$ and $\Delta H_{ad,i}^0$ are the standard entropy and ethalphy of adsorption, respectively, for compound i. The results of fitting the experimental data are shown in Fig. 6, and the enthalpies and entropies of adsorption for hydrogen and acetic acid obtained from the temperature dependence of K_{H_2}, K_{Ac}, and $K_A K_{Ace}$ are reported in Table 6. The rate expression derived from this model gave a mean residual sum of squares (MRSQ) of its predicted rates equal to 0.005, which was half that obtained from the rejected model (29). Note that Eqs. [4] and [5] can be combined to describe dissociative HOAc adsorption to form a surface acetate species. The enthalpy and the entropy of adsorption for HOAc and hydrogen are negative, as required by thermodynamics, and the entropy for HOAc adsorption on either Fe^0 or FeO surfaces satisfies additional constraints and guidelines for evaluating the entropy of adsorption, i.e., (53, 54)

$$0 < |\Delta S^0| < S_g^0, \quad [18]$$

$$10 \le -\Delta S^0 \le 12.2 - 0.0014 * \Delta H^0, \quad [19]$$

where S_g^0 is the absolute entropy of HOAc or hydrogen in the gas phase. The absolute entropies for HOAc and H_2 at 500 K are 77 (55) and 34 e.u. (56), respectively; thus the entropy of adsorption for H_2 is still somewhat greater than the maximum allowed, but the uncertainty of the ΔS_{ad}^0 value obtained from extrapolating the two 95% confidence limits is quite large at ±170 e.u. The heat of adsorption for H_2 is at the high end of the range of values reported for H_2 on polycrystalline Fe metal (39–43), implying that only

TABLE 6

Enthalpies and Entropies of Adsorption from Parameters in Rate Expression [16]

Adsorption step	ΔH_{ad}^0 (kcal/mol)	ΔS_{ad}^0 (cal/mol/K)
H_2 on Fe^0 (K_{H_2})	−33	−43
Acetic acid on Fe^0 (K_{Ac})	−26	−18
Acetic acid on FeO ($K_A K_{Ace}$)	−8	−10

Note. Standard state, 1 atm.

the high-energy sites are involved under reaction conditions. These results also imply that dissociative acetic acid adsorption on an iron oxide surface is much weaker than that on metallic iron.

The above reaction model was derived assuming a uniform catalyst surface throughout the catalyst bed; however, the state of the iron surfaces may vary with reactant (and product) partial pressures, i.e., the reduction potential of the gas phase, particularly at high temperatures. If the number of active sites were to vary with the H_2 pressure because of either the Fe/FeO redox potential or coverage by carbonaceous species, a higher dependency on P_{H_2} could result (57), and this could explain the high dependency at higher temperatures. To what extent this situation occurred and affected catalytic behavior under the reaction conditions applied here is not yet known and further work is required to examine and to quantify possible changes of the Fe surface. Such a study could also provide more information about the observed particle size effects, which are tentatively attributed to the state of the iron surface under reaction conditions.

SUMMARY

The catalytic behavior of vapor-phase acetic acid hydrogenolysis and hydrogenation was studied over both supported and unsupported iron with metal crystallite sizes ranging from 10 to 4000 nm. Very high selectivity to acetaldehyde (above 90%) was obtained at low conversion, but this dropped to ~80% as conversions approached 40%. In addition to conversion, temperature and hydrogen partial pressure also affected the selectivity. The iron crystallite size has a significant effect on both the TOF for reduction by H_2 and the apparent activation energy, as the former increased and the latter decreased as Fe crystallite size increased. Acetic acid reduction over iron catalysts was described by a model invoking two types of sites, i.e., one set on metallic Fe and the other on Fe oxide, and the kinetics at steady state were modeled by a Langmuir–Hinshelwood-type mechanism invoking adsorbed hydrogen atoms on the metallic sites and an acetate species adsorbed on the oxidic sites as the predominant intermediate species, with addition of the second H atom to form adsorbed acetaldehyde being the rds.

ACKNOWLEDGMENT

This study was sponsored by the DOE, Division of Basic Energy Sciences, via Grant DE-FG02-84ER13276.

REFERENCES

1. Gerhartz, W., Yamamoto, Y. S., Campbell, F. T., Pfefferkorn, R., and Rounsaville, J. F., Eds., "Ullman's Encyclopedia of Industrial Chemistry," 5th Ed. VCH, Weinheim, 1985.
2. Rosemund, K. W., *Ber. Dtsch. Chem. Ges.* **51**, 585 (1918).
3. Zakharin, L. I., and Khorlina, I. M., *Tetrahedron Lett.* 619 (1962).
4. Weissman, P. M., and Brown, H. C., *J. Org. Chem.* **31**, 283(1966).
5. Kanazawa, R., and Tokoroyama, T., *Synthesis* 526 (1976).
6. Brown, H. C., *Tetrahedron* **35**, 567 (1979).
7. Brown, H. C., and Tsukamoto, A., *J. Am. Chem. Soc.* **86**, 1089 (1964).
8. Izawa, T., and Mukaiyama, T., *Bull. Chem. Soc. Jpn.* **52**, 555. (1979).
9. Brown, H. C., Cha, J. S., Yoon, N. M., and Nazer, B., *J. Org. Chem.* **52**, 5400 (1987).
10. Woodham, J. F., and Holland, C. D., *Ind. Eng. Chem.* **52**, 985 (1991).
11. Mann, R. S., and Rouleau, E., *in* "Symp. Selective Oxidation Processes, Chicago," p. 46. Am. Chem. Soc., Washington, DC, 1964.
12. Brettle, R., *in* "Comprehensive Organic Chemistry" (J. F. Stoddart, Ed.), Vol. 1, p. 1105. Pergamon, Oxford, 1979.
13. Rachmady, W., and Vannice, M. A., *J. Catal.* **192**, 322 (2000).
14. Pestman, R., Koster, R. M., and Ponec, V., *Recl. Trav. Chim. Pays-Bas* **113**, 426 (1994).
15. Grootendorst, E. J., Pestman, R., Koster, R. M., and Ponec, V., *J. Catal.* **148**, 261 (1994).
16. Tustin, G. C., Depew, L. S., and Collins, N. A., U.S. Patent 6,121,498 (2001).
17. Yokohama, T., Fujita, N., and Maki, T., U.S. Patent 5,306,845 (1994).
18. Jacquot, R., LeClercq, J.-M., Mercier, C., and Popa, J.-M., U.S. Patent 5,973,210 (1999).
19. Pestman, R., Koster, R. M., Boellaard, E., van der Kraan, A. M., and Ponec, V., *J. Catal.* **174**, 142 (1998).
20. Cressely, J., Farkhani, D., Deluzarche, A., and Kiennemann, A., *Mater. Chem. Phys.* **11**, 413 (1984).
21. Carter, J. L., and Savini, C. G., U.S. Patent 3,472,794 (1969).
22. Chen, A., Kaminsky, M., Geoffroy, G. L., and Vannice, M. A., *J. Phys. Chem.* **90**, 4810 (1986).
23. Topsøe, H., Topsøe, N., Bohlbro, H., and Dumesic, J. A., *in* "Proceedings, 7th International Congress on Catalysis, Tokyo, 1980" (T. Seiyama and K. Tanabe, Eds.), p. 247. Elsevier, Amsterdam, 1980.
24. Emmett, P. H., and Brunauer, S., *J. Am. Chem. Soc.* **59**, 319 (1937).
25. Boudart, M., Delbouille, A., Dumesic, J. A., Khammouma, S., and Topsøe, H., *J. Catal.* **37**, 486 (1975).
26. Jung, H.-J., Vannice, M. A., Mulay, L. N., Stanfield, R. M., and Delgass, W. N., *J. Catal.* **76**, 208 (1982).
27. Madon, R. J., and Boudart, M., *Ind. Eng. Chem Fundam.* **21**, 438 (1982).
28. Weisz, P. B., *Z. Phys. Chem.* **11**, 1 (1957).
29. Rachmady, W., Ph.D. thesis. The Pennsylvania State University, University Park, PA, 2001.
30. Yoon, K. J., Walker, P. L., Jr., Mulay, L. N., and Vannice, M. A., *Ind. Eng. Chem. Prod. Res. Dev.* **22**, 519 (1983).
31. Farrauto, R. J., *AIChE Symp. Ser.* **70**, 163 (1974).
32. Stencel, J. M., Rao, V. U. S., Diehl, J. R., Rhee, K. R., Dhere, A. G., and DeAngelis, R. J., *J. Catal.* **84**, 109 (1983).
33. Emmett, P. H., and Takezawa, N., *J. Hokkaido Inst. Catal.* **26**, 37 (1978).
34. Gregg, S. J., and Sing, K. S. W., *in* "Adsorption, Surface Area and Porosity," 2nd ed., p. 76 Academic Press, New York, 1982.
35. Rachmady, W., and Vannice, M. A., *J. Catal.* **208**, 170 (2002).
36. Niemantsverdriet, J. W., van der Kraan, A. M., van Loef, J. J., and Delgass, W. N., *J. Phys. Chem.* **87**, 1292 (1983).
37. (a) Pestman, R., Ph.D. thesis, Leiden University, 1995; (b) Pestman, R., Koster, R. M., Pieterse, J. A. Z., and Ponec, V., *J. Catal.* **168**, 255 (1997).
38. Martinez, R., Huff, M. C., and Barteau, M. A., *Appl. Catal. A* **200**, 79 (2000).
39. Wedler, G., Geuss, K.-P., Colb, K. G., and McElhiney, G., *Appl. Surf. Sci.* **1**, 471 (1978).
40. Beeck, O., Cole, W. A., and Wheeler, A., *Discuss. Faraday Soc.* **8**, 314 (1950).

41. Wahba, M., and Kemball, C., *Trans. Faraday Soc.* **49**, 1351 (1953).
42. Klemperer, D. F., and Stone, F. S., *Proc. R. Soc. London Ser. A* **243**, 375 (1957).
43. Cerny, S., and Ponec, V., *Catal. Rev.* **2**, 249 (1968).
44. Sen, B., Chou, P., and Vannice, M. A., *J. Catal.* **101**, 517 (1986), and references therein.
45. Bradley, T. L., and Stickney, R. E., *Surf. Sci.* **38**, 313 (1973).
46. Kock, A. J. H. M., and Geus, J. W., *Prog. Surf. Sci.* **20**, 165 (1985).
47. Dumesic, J. A., Topsøe, H., Khammouma, S., and Boudart, M., *J. Catal.* **37**, 503 (1975).
48. (a) Storm, D., and Boudart, M., *in* "6th North American Catalysis Society Meeting, Chicago." Paper G5. March, 1979; (b) Storm, D., Ph.D. dissertation. Stanford University, Stanford, CA, 1978.
49. Boudart, M., *Adv. Catal. Relat. Subjects* **20**, 153 (1969).
50. Vink, T. J., Der Kinderen, J. M., Gijzeman, O. L. J., and Geus, J. W., *Appl. Surf. Sci.* **26**, 367 (1986).
51. Vink, T. J., Sas, S. J. M., Gijzeman, O. L. J., and Geus, J. W., *J. Vac. Sci. Technol. A* **5**, 1028 (1987).
52. Rachmady, W., and Vannice, M. A., submitted for publication.
53. Boudart, M., *AIChE J.* **18**, 465 (1972).
54. Vannice, M. A., Hyun, S. H., Kalpacki, B., and Liauh, W. C., *J. Catal.* **56**, 358 (1979).
55. Chao, J., Hall, K. R., Marsh, K. N., and Wilhoit R. C., *J. Phys. Chem. Ref. Data* **15**, 1369 (1986).
56. Cox, J. D., Wagman, D. D., and Medvedev, V. A., Eds., "Codata Key Values for Thermodynamics." Hemisphere, Washington, DC/ New York 1989.
57. Gault, F. G., *Adv. Catal.* **30**, 1 (1981).